

The Hemodynamic Comparative Study Between Pulsatile and Non-Pulsatile VA ECMO: A Primary Numerical Study

Qi Zhang¹, Bin Gao¹, Yue Shi¹ and Chang Yu^{1, *}

Abstract: Although pulsatile ECMO, as novel kinds of ECMO, has been attracted more and more attention, the differences of the hemodynamic effects of the pulsatile ECMO on the aorta, the cerebral perfusion, and left ventricular work were still under-investigated. The aim of this study was to clarify the hemodynamic differences of the cardiovascular system between the pulsatile and non-pulsatile VA ECMO. In this study, three ECMO support modes, named as “constant flow mode”, “co-pulse mode” and “counter pulse mode”, were designed. The computational fluid dynamics (CFD) study was carried out. The distribution of the oxygenated blood, the blood velocity vector, the oscillatory shear index (OSI), the relative residence time (RRT), the left ventricular external work (EW), the equivalent left ventricular afterload (EAL) and the energy loss of cardiovascular system (EL) were calculated to compare the hemodynamic differences. The simulation results demonstrate that the oxygenated blood under co-pulse mode was easier to perfuse into the three branches vessels than that under both other modes. In addition, the ECMO under counter pulse mode could also achieve lowest RRT (constant flow mode 220 vs. co-pulse mode 132 vs. counter pulse mode 93). Similarly, the ECMO under counter pulse mode could significantly reduce the left ventricular external work (co-pulse mode 1.51 w vs. constant flow mode 1.44 w and counter pulse mode 1.30 w), left ventricular afterload (constant flow mode 1.03 mmHg·s/ml vs. co-pulse mode 1.67 mmHg·s/ml vs. counter pulse mode 0.82 mmHg·s/ml) and energy loss of arterial system (constant flow mode 0.18 w vs. co-pulse mode 0.50 w vs. counter pulse mode 0.16 w). In short, the ECMO under counter pulse mode could have advantages to the left ventricular unloading. In contrast, the ECMO under co-pulse mode has more benefit to cerebral oxygen perfusion.

Keywords: pulsatile, non-pulsatile, VA ECMO, hemodynamics, CFD.

1 Introduction

Venoarterial Extracorporeal membrane oxygenation (VA ECMO) provided emergency mechanical circulatory assistance to patients with cardiogenic shock refractory to medical therapies [Extracorporeal Life Support Organization (2013)]. The pulsatile ECMO, which could generate pulsatile blood flow by changing the rotational speed of the blood pump, was attracted more and more attention, as it could potentially reduce systemic vascular resistance, protect the microcirculatory function, as well as improve the catecholamine response, splanchnic perfusion, cerebral perfusion, and myocardial blood flow [Guan,

¹ School of Life Science and BioEngineering, Beijing University of Technology, Beijing, 100124, China.

* Corresponding Author: Chang Yu. Email: changyu@bjut.edu.cn.

Karkhanis, Wang et al. (2010); Trummer, Foerster, Buckberg et al. (2014)]. For instance, Adedayo et al. [Adedayo, Wang, Kunselman et al. (2014)] reported that pulsatile ECMO could provide more dynamic energy to the circulatory system than non-pulsatile ECMO. Wang et al. [Wang, Kunselman, Clark et al. (2015)] demonstrated that the novel pulsatile ECMO could achieve better hemodynamic energy transmission. Similarly, Wolfe et al. [Wolfe, Strother, Wang et al. (2015)] found that pulsatile flow improved the transmission of hemodynamic energy to the patient without significantly affecting the pressure drops across the circuit. Although the above-mentioned studies demonstrated that the pulsatile ECMO could achieve better performance on energy transmission, its precise hemodynamic effects on the aorta, the cerebral perfusion, and left ventricular work were still under-investigated.

Computational fluid dynamic (CFD) has become an important method for clarifying the hemodynamic states of ECMO. For instance, Zhang et al. [Zhang, Gao and Chang (2018)] studied the distribution of the aortic oxygenated blood under VA ECMO. Gu et al. [Gu, Zhang, Gao et al. (2016)] compared the hemodynamic differences between the central ECMO and peripheral ECMO, by using CFD approach. Caruso et al. [Caruso, Gramigna, Serraino et al. (2015)] studied the influence of aortic outflow cannula orientation on aortic blood flow pattern during central ECMO, by using CFD method. Similarly Assmann et al. [Assmann, Gül, Benim et al. (2015)] evaluated the hemodynamic advantages of novel dispersive aortic cannulas on the distribution of aortic wall shear stress. Although CFD approach was widely applied to evaluate and optimize the hemodynamic state of ECMO, there was no study on the hemodynamic effects of pulsatile ECMO on the aortic hemodynamics, the cerebral perfusion, and the left ventricular work.

In order to study the hemodynamic effects of pulsatile ECMO, numerical studies, based on patient-specific arterial geometric model with three different boundary conditions (named as “constant flow mode”, “co-pulse mode” and “counter pulse mode”, respectively), were conducted. The computational fluid dynamic (CFD) theory was employed to calculate the arterial hemodynamic states. The distribution of oxygenated blood and deoxygenated blood, the blood velocity vector, oscillatory shear index (OSI), relative residence time (RRT), the left ventricular external work (EW), the equivalent left ventricular afterload (EAL) and the energy loss of cardiovascular system (EL) were chosen as the indicators to evaluate the hemodynamic effect caused by pulsatile ECMO.

2 Material and methods

2.1 Arterial model reconstruction

In order to evaluate the hemodynamic states, a patient-specific arterial model was established based on computed tomography angiography (CTA) data, obtained from a healthy volunteer. The volunteer was 26-year old healthy man, who was not suffered from any cardiovascular disease. The healthy volunteer was chosen to ensure the scalability of the study. The model consisted of the ascending aorta, aortic arch, brachiocephalic artery, left common carotid artery, left subclavian artery, descending aorta and femoral artery (Fig. 1A). Written informed consent was obtained from the volunteer for using medical images in the study. The 3D arterial geometric model was

constructed by using these data and by using commercial 3D reconstruction software MIMICS (Materialise, Belgium). And then, the model was transferred into the commercial software Geomagic (Geomagic, USA) to improve its surface quality (Fig. 1A).

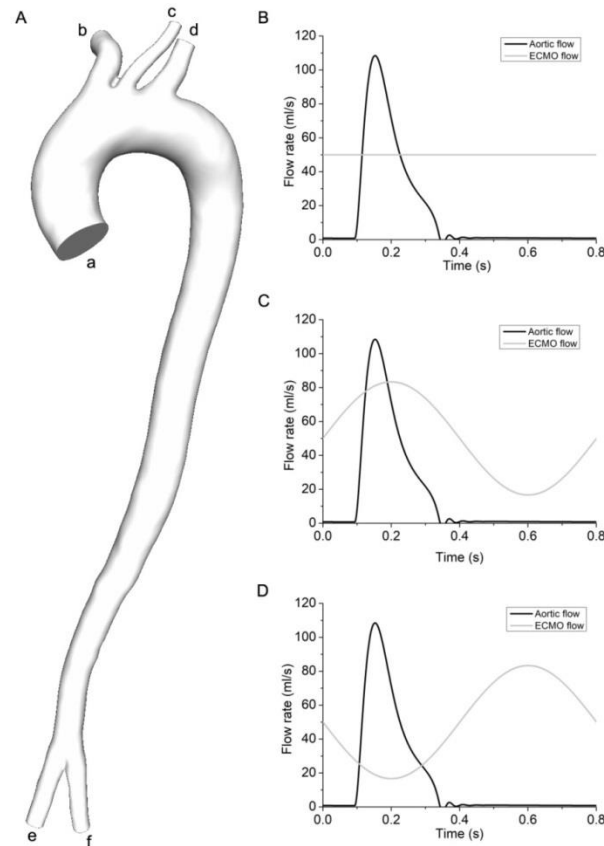


Figure 1: The geometric model of artery system and boundary conditions of three modes. 1A was the geometric model of arterial system. In the 1A, a denoted the ascending aorta, b represented the brachiocephalic artery, c was the left common carotid artery, d denoted the left subclavian artery, e and f represented the left and right femoral artery. 1B illustrated the boundary condition of constant flow mode; 1C showed the boundary condition of co-pulse mode, 1D illustrated the boundary condition of counter pulse mode

2.2 Meshing generation

The arterial geometric models were meshed by using the commercial package Hexpress (NUMECA, Belgium), which could generate high quality unstructured hexahedral grids, and then sent into CFD package FLUENT (ANSYS, Canonsburg, PA, USA). In order to determine the appropriate numbers of elements for this model, grid independency tests, targeting the blood velocity contour as measures, were conducted. The results confirmed that 2.4 million hexahedral elements are sufficient for this study. In order to obtain more

accuracy results, 12 boundary layers, in which the stretching ratio was 1.2, were employed (Fig. 2).

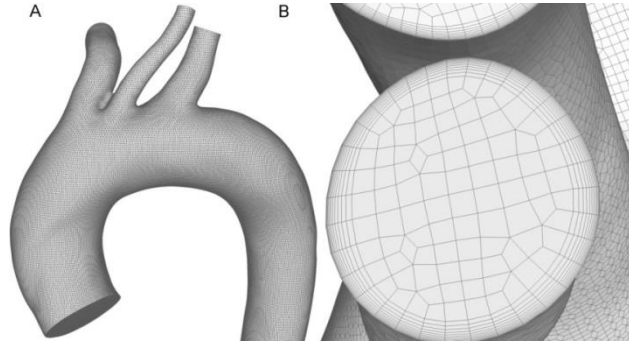


Figure 2: The optimal mesh, nearly 2.4 million elements. 2A shows the hexahedral grids of the geometric model; 2B illustrated the boundary layers

2.3 Numerical approaches

The flow was governed by the mass and momentum conservation for incompressible fluid, known as the Continuity and Navier-Stokes Eqs. (1) and (2) [Kabinejadian, Chua, Ghista et al. (2010)].

$$\nabla \cdot \mathbf{u} = 0 \quad (1)$$

$$\rho \frac{\partial \mathbf{u}}{\partial t} + \rho(\mathbf{u} \cdot \nabla) \mathbf{u} = -\nabla p + \mu \nabla^2 \mathbf{u} \quad (2)$$

where \mathbf{u} was blood velocity, t represented the time, and p denoted the blood pressure, ρ and μ was the density and the dynamic viscosity of the blood, respectively. The Eqs. (1) and (2) were solved by ANSYS/Fluent 16.2, in which the finite volume-based pressure-correction algorithm and second-order upwinding scheme were selected.

2.4 Boundary conditions

According to the clinical practice, the hemodynamic states of artery under pulsatile and non-pulsatile ECMO were study. In all studies, the left femoral artery was chosen as the inlet, to where the outflow cannula of ECMO was inserted. And the diameter of the ECMO outflow cannula was assumed to be the same with that of left femoral artery. The non-pulsatile ECMO, which is the conventional ECMO used in the clinical practice, was used as the reference. In the non-pulsatile mode, the physiological velocity data (mean flow rate was 1 L/min) was used as the boundary of aortic root. And a constant flow rate, which was set as 3 L/min, was used as the inlet boundary condition of ECMO (Fig. 1B). For pulsatile ECMO, there are two types, named as co-pulse mode and counter pulse mode, were designed. For co-pulse mode, the blood flow from ECMO synchronized with the physiological blood flow jetted from aortic root (Fig. 1C). In addition, the blood flow, jetted from counter pulse ECMO, has 180 degree phase delay with the physiological blood flow, pumped from aortic root (Fig. 1D). In three studies, the physiological blood flow was derived from a lumped parameter model, of which the accuracy is validated by

clinical data [Gao, Chang, Xuan et al. (2013)]. To mimic the physiological condition of patient, supported by ECMO, the mean value of blood flow, imposed at the aortic root, was reduced to 1 L/min. Under co-pulse ECMO case, the blood flow, jetted from ECMO, was denoted as the Eq. (3).

$$flow_{copulse} = 3 + 2 * \sin\left(\frac{2 * \pi * t}{T}\right) \quad (3)$$

Where $flow_{copulse}$ was the blood flow, whose unit was L/min. T represented the cardiac cycle, t was the time step. The second mode was named as counter pulse mode. In this mode, the blood flow, jetted from ECMO, had 180 degree phase delay with the blood flow pumped from aortic root. It was denoted as the Eq. (4).

$$flow_{counterpulse} = 3 - 2 * \sin\left(\frac{2 * \pi * t}{T}\right) \quad (4)$$

Where $flow_{counterpulse}$ was the blood flow, jetted from ECMO. Its unit was L/min. The third mode was named as constant flow mode, in which the blood flow, jetted from ECMO, was set at 3 L/min. Moreover, the constant blood pressure, used as the boundary conditions, was imposed at the outlet of three branch vessels (80 mmHg) and the left femoral artery (70 mmHg) [Yu, Liu, Wong et al. (2016)]. And the cardiac cycle was set to 0.8 s.

2.5 Calculation settings

The blood was assumed as the incompressible, homogeneous and Newtonian fluid, of which the viscosity and density is set 0.0035 Pa*s [Khalafvand, Ng, Zhong et al. (2012)] and 1050 kg/m³ [Zhao, Liu, Bai et al. (2012)], respectively. The cardiac cycle was set to be 0.8 s and the time step was 0.01 s. According to the geometric size of the geometric model, the blood density and the peak systolic velocity of blood, the peak systolic Reynolds number Re was larger than 3500. Hence, the SST k-w turbulence model, which was confirmed to fit for illustrating the turbulence flow states in the aorta [Cheng, Tan, Riga et al. (2010)], was used in this study. The backward Euler implicit time integration algorithm was employed with a fixed time step (0.01 s). 5 cardiac cycles were calculated to eliminate the effect of initial conditions and the hemodynamic parameters in the 5th cardiac cycles were extracted for hemodynamic analysis. The convergence criterion in this study was set to be 10^{-3} .

2.6 Hemodynamic analysis

In order to evaluate the hemodynamic differences between pulsatile and non-pulsatile ECMO, OSI, RRT, EW, EAL and EL were calculated in this study. The EW was an important factor for quantifying the left ventricular load [Gao, Chang, Xuan et al. (2013)]. It was described as the Eq. (5)

$$EW(t) = 0.0022 * CO(t) * AOP(t) \quad (5)$$

Where $EW(t)$ was the external work of the left ventricle (watts), $AOP(t)$ represented the pressure at the aortic root (mmHg), $CO(t)$ denoted the cardiac output (L/min).

According to Moscato's work, the left ventricular EAL, which was an important factor

for evaluating the left ventricular afterload, was the ratio of the instantaneous aortic pressure and cardiac output. It denoted as the Eq. (6)

$$EAL = \frac{1}{T} \int_0^T \left(\frac{AOP(t)}{CO(t)} \right) dt \quad (6)$$

Where EAL was the equivalent afterload of the left ventricle (mmHg·s/ml), T represented the cardiac cycle (s), $AOP(t)$ denoted the instantaneous aortic pressure (mmHg), $CO(t)$ was the instantaneous cardiac output (ml/s).

Energy loses (EL) was a very important factor, which reflected the efficiency of energy transmission. According to the theory of conservation of hemodynamic energy, the EL was described as the equation

$$EL(t) = 0.0022 * (AOP(t) * CO(t) + P_E(t) * F_E(t) - \sum_k P_k(t) * F_k(t)) \quad (7)$$

Where $EL(t)$ represented the energy lose (watts), $AOP(t)$ represented the pressure at the aortic root (mmHg), $CO(t)$ denoted the cardiac output (L/min), $P_E(t)$ described the pressure at the inlet of left femoral artery (mmHg), $F_E(t)$ represented the blood flow at the inlet of left femoral artery (L/min), $P_k(t)$ and $F_k(t)$ were the pressure (mmHg) and blood flow (L/min) of three branches vessel and left femoral artery, k included the brachiocephalic artery, left common carotid artery, left subclavian artery and left femoral artery.

OSI was defined as the equation

$$OSI = 0.5 * \left(1 - \frac{\left| \int_0^T \tau_w dt \right|}{\int_0^T |\tau_w| dt} \right) \quad (8)$$

RRT [Rikhtegar, Knight, Olgac et al. (2012)] was defined as the Eq. (9)

$$RRT = \frac{1}{(1 - 2 * OSI) * TAWSS} \quad (9)$$

3 Results

In order to evaluate the hemodynamic differences between pulsatile ECMO and non-pulsatile ECMO on artery system, the distribution of OSI, RRT and the change in EW and EL respect time steps were shown in Figs. 3-7. Four special time points (0.10 s, 0.15 s, 0.2 s and 0.60 s) were chosen to evaluate hemodynamic states. 0.10 s was the time point, when the blood begins to jet from the aortic root. 0.15 s was the time point, when the left ventricle output reached its maximum value. 0.20 s was the time, when the blood flow, from co-pulse mode of ECMO, reached its peak value. Similarly, 0.60 was the time point, when the co-pulse ECMO output velocity reached its minimum values.

3.1 The distribution of oxygenated and deoxygenated blood

Fig. 3 illustrated the change in the distribution of oxygenated (the light gray streamline) and deoxygenated (the dark gray streamline) blood under support of three modes, during the whole cardiac cycle. It was found that before ejection phase, the oxygenated blood flow, under co-pulse mode ECMO support, easier entered into the brachiocephalic artery, left common carotid artery and left subclavian artery than that under conventional

constant mode (region a, at 0.1 s). In contrast, under counter pulse mode, the oxygenated blood flow from ECMO was difficult to flow into the three branches vessel. During the ejection phase, the deoxygenated blood flow, entering into the three branches vessel, gradually increased. At the peak systole ($t=0.15$ s), three braches vessels were totally perfused by deoxygenated blood flow under three modes. And then the percentage of oxygenated blood, flowing into the three braches vessels, was gradually increased under co-pulse ECMO mode, as the increase of ECMO flow rate. At the peak time of ECMO flow rate under co-pulse mode ($t=0.2$ s), the three braches vessels was perfused by the mixed blood (oxygenated blood and deoxygenated blood) under co-pulse mode (region b), while they were perfused by deoxygenated blood under other two modes. In the diastolic phase, the three braches vessels were totally perfused by oxygenated blood, from ECMO, as the blood flow, pumping from left ventricle, was reduced appropriate to 0 L/min (region c).

3.2 The aortic flow pattern

The blood flow pattern under three modes was demonstrated in Fig. 4. At the beginning of the ejection phase, the oxygenated blood from ECMO and the deoxygenated blood from the left ventricle were mixed at the aortic arch (region a, at 0.1 s). And the stagnant area was observed at the inner wall of the aortic arch under all modes. At the peak time of ECMO flow rate under co-pulse mode ($t=0.2$ s), the oxygenated blood from co-pulse ECMO could retrograde from femoral artery to aorta (region b). And during the diastolic phase, the turbulence flow and vortex were observed at the ascending aorta (region c).

3.3 The distribution of OSI and RRT

Fig. 5 illustrated the distribution of OSI under three modes. It was seen that the peak value of OSI were observed at the inner wall of the aortic arch and descending aorta (region a: Constant flow mode 0.44 vs. co-pulse mode 0.46 vs. counter pulse mode 0.45; region b: Constant flow mode 0.39 vs. co-pulse mode 0.44 vs. counter pulse 0.45). In addition, the area of high OSI under counter pulse mode was smaller than that under co-pulse mode ECMO (region a and b). Fig. 6 showed the distribution of RRT under three modes. It is seen that the high RRT region were observed at the inner wall of aortic arch (region a: Constant flow mode 220 vs. co-pulse mode 132 vs. counter pulse mode 93), the outer wall of the beginning of the descending aorta (region b: Constant flow mode 21 vs. co-pulse mode 27 vs. counter pulse mode 19) and the inner wall of the descending aorta (region c: Constant flow mode 19 vs. co-pulse mode 36 vs. counter pulse mode 18). Among the three modes, RRT, obtained from co-pulse mode, was much higher than that obtained from constant flow mode and counter pulse mode (region a, b and c). Moreover, at aortic arch, the area of the high RRT region at co-pulse mode was significantly larger than that under constant flow mode and counter flow mode (region a).

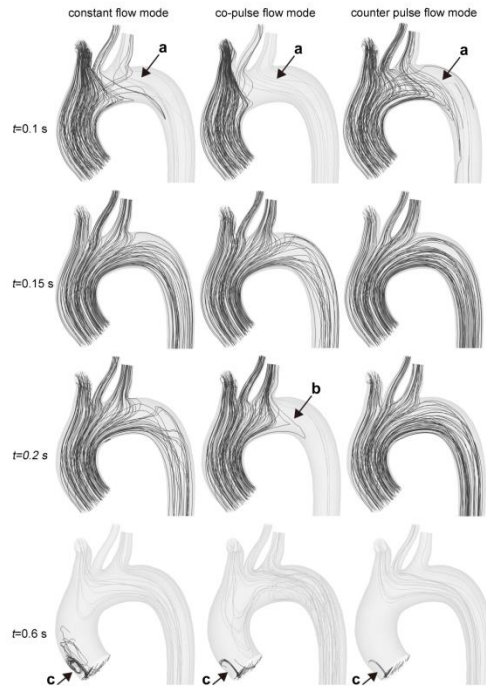


Figure 3: The distribution of oxygenated blood flow and deoxygenated blood flow at aortic arch

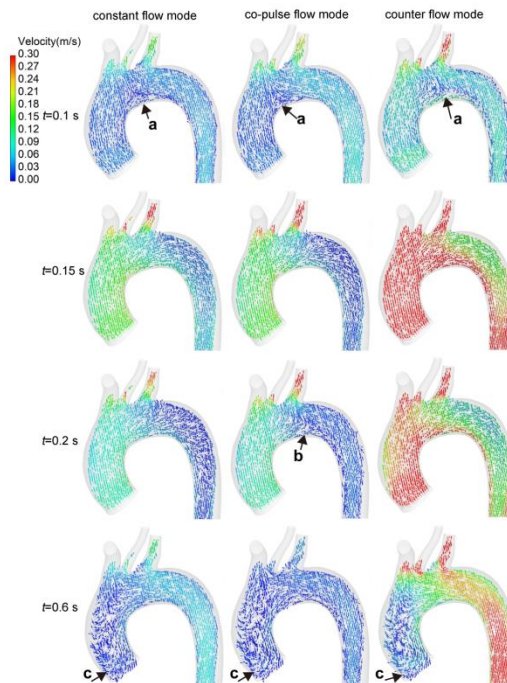


Figure 4: The distribution of blood velocity vector under three modes

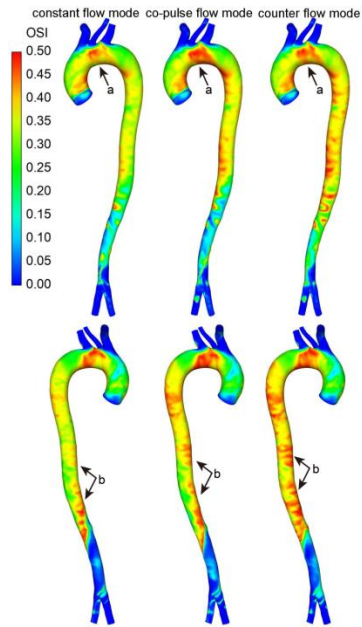


Figure 5: The distribution of OSI under three modes

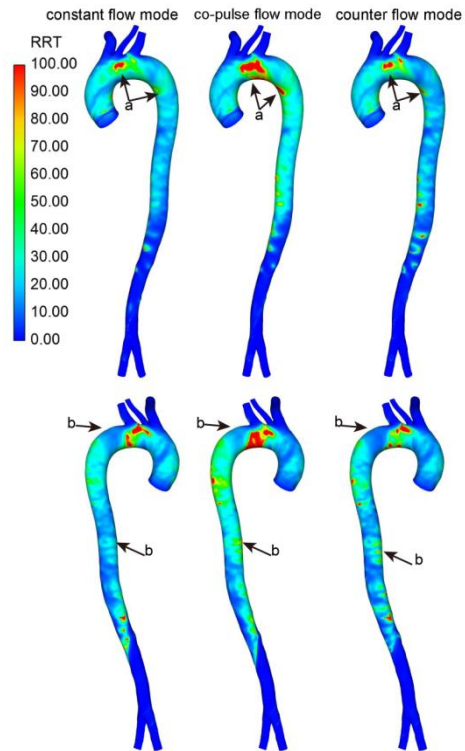


Figure 6: The distribution of RRT under three modes

3.4 The changes in EW, EAL and EL

Fig. 7 illustrated the comparison results of EW, EAL and EL under three ECMO modes. Fig. 7A illustrated the change in EW under three cases. It was seen that, under three ECMO modes, EW significantly increased in the ejection phase. And then, it reduced to zero during the diastolic phase, as the flow rate through the aortic root is zero. In addition, the peak value of EW, under co-pulse ECMO support was the highest one than other two modes (co-pulse mode 1.51 w vs. constant flow mode 1.44 w and counter pulse mode 1.30 w). Moreover, EW, under counter pulse mode, slightly reduced compared with constant flow mode. Fig. 7B showed the EAL under three modes. The EAL, under counter pulse ECMO support, achieve the minimum value (constant flow mode 1.03 mmHg·s/ml vs. co-pulse mode 1.67 mmHg·s/ml vs. counter pulse mode 0.82 mmHg·s/ml). The change in EL of three modes was demonstrated in Fig. 7C. It was found that the EL was changed along with the left ventricular motion. When the left ventricle contracted to pump the blood into the aorta, the EL of the circulatory system was significantly increased, while it rapidly reduced during the diastolic phase. Among the all modes, co-pulse mode could achieve the highest EL (constant flow mode 0.18 w vs. co-pulse mode 0.50 w vs. counter pulse mode 0.16 w) at peak systole ($t=0.13$ s).

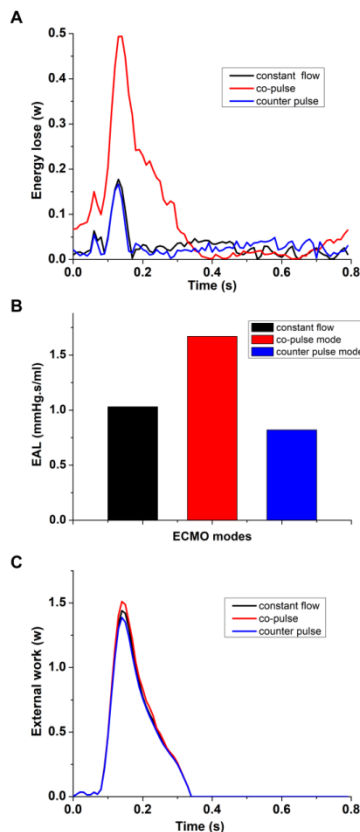


Figure 7: The changes in EW, EAL and EL under three ECMO modes. 7A shows

changes in the left ventricular external work during the whole cardiac cycle; 7B illustrates the difference of EAL between three modes; 7C is the changes in EL respecting with time under three modes

4 Discussion

In this study, we analyzed the hemodynamic changes caused by pulsatile ECMO and non-pulsatile ECMO. Both pulsatile and non-pulsatile ECMO resulted in the enhancement of OSI and RRT. Moreover, the co-pulse mode ECMO achieved higher OSI, RRT, EW, EAL and EL, compared with other two modes. This was the first study that comparing the hemodynamic differences between conventional constant flow ECMO, co-pulse mode ECMO and counter pulse mode ECMO.

VA-ECMO became an alternative method for life threatening circulatory failure with or without respiratory failure [Lindfors, Frenckner, Sartipy et al. (2017)]. Arterial desaturation in the upper body was frequently seen in patients with VA-ECMO [Alwardt, Patel, Lowell et al. (2013)]. The reason of this phenomenon was assumed that blood leaving the ECMO was fully saturated with oxygen, but usually only reaches the descending aorta and the distal aortic arch [He and Ku (1996)]. This hypothesis could be proven by the results of this study. In this study, the mixture of deoxygenated blood from left ventricle and the oxygenated blood from ECMO was observed (Fig. 3). At the beginning of ejection phase, the deoxygenated blood and oxygenated blood was mixed at the aortic arch. And the three braches was perfused by the mixture blood, in which the oxygen saturation was reduced. And then, along with the increase of deoxygenated blood flow, the percentage of deoxygenated blood, flowing into the three braches vessels, was gradually increased. At the peak systole, the three braches vessels were totally perfused by deoxygenated blood flow. Among the three different modes, the perfusion pattern is totally different from each other. Compared with co-pulse mode, the deoxygenated blood, under counter pulse mode, easier flow into the ascending aorta (Fig. 4 0.2 s). In contrast, during the diastolic phase, under counter pulse mode, much more oxygenated blood flow entered into the three braches vessels (Fig. 4 0.6 s). This was due to the oxygenated blood flow rate increased during diastolic phase. In addition, the duration of diastolic phase was longer than systolic phase; hence, the ECMO under counter pulse mode could provide better perfusion performance than that under co-pulse mode and constant flow mode.

Hemodynamic factors were believed to play important roles in the vascular dysfunction. OSI was an important hemodynamic factor that highlighted areas where the wall shear stress vector presents directional changes over the cardiac cycle [He (1996)]. Many studies supported that OSI could strong effect on vascular functions. For instants, Wen et al. [Wen, Yang, Tseng et al. (2010)] reported that the over high OSI value tended to cause the dysfunction of endothelial cell of arterial system. Similarly, Goubergrits et al. [Goubergrits, Kertzscher, Schoneberg et al. (2008)] reported that OSI values of greater than 0.2 represented detrimental flow conditions that could be prone to the development of atherosclerosis and thrombosis. In this study, high OSI value regions were observed both under pulsatile ECMO and non-pulsatile mode ECMO support (Fig. 4). That meant that both pulsatile and non-pulsatile ECMO may contribute to vascular dysfunction, which was consistent with the clinical practice [Bisdas, Beutel, Warnecke et al. (2011)].

From the results of this study, high OSI may result from the variation of the instantaneous value of left ventricular outflow. Along with the increase of left ventricular outflow rate, the location, where the left ventricular outflow contracted with the blood flow from ECMO, was moved toward to the descending aorta. In contrast, during the diastolic phase, this mixed location was moved toward to the ascending aorta. Among the three modes, OSI value in co-pulse mode was significantly higher than constant flow mode and counter pulse mode. That means compared with constant flow mode and counter pulse mode, ECMO, working under co-pulse mode, could provide worse hemodynamic conditions to arterial system. RRT was another important hemodynamic factor that indicated the particles stay near the wall [Pinto and Campos (2016)]. RRT should be between 0 and infinite, for zones with close recirculation. According to Lee's study, the RRT values higher than 8 should be considered elevated. High RRT values indicated potential zones of thrombosis and deposition appearance, as verified by Morbiducci et al. [Morbiducci, Gallo, Massai et al. (2011)] and Sousa et al. [Sousa, Castro, António et al. (2016)]. In this study, it was found that the high RRT area was observed at aortic arch and descending aorta. And the value and area of high RRT was much larger than that obtained from compared with constant flow mode and counter pulse mode. In short, the co-pulse mode ECMO may provide worse hemodynamic state to the arterial system than that obtained from both other modes.

Currently, the effects of ECMO on the left ventricular function and afterload has been attracted much more interests. Reesink et al. [Reesink, Sauren, Dekker et al. (2005)] found that the myocardial oxygen consumption was significantly increased at the systolic phase. Similarly, Cheyppesh et al. [Cheyppesh, Yu, Li et al. (2014)] reported that the myocardial oxygen consumption was increased along with the increase of ECMO flow rate. These findings were consistent with our results. In this study, EW was used to evaluate the left ventricular work, which was related to the myocardial oxygen consumption. It was seen that EW was varied along with the cardiac motion. During the systolic phase, EW rapidly increased. And among the three modes, EW, obtained from co-pulse mode ECMO, was the largest one. Similarly, EAL was another hemodynamic factor for evaluating the left ventricular working condition. It was confirmed that the increase of EAL resulted in the increase of myocardial oxygen consumption. And reduction of the EAL became an important aim for protecting and promoting cardiac function. In this study, it was found that EAL, under three modes, was totally different from each other. EAL, obtained from co-pulse mode ECMO, was the largest among the three modes, while the EAL, under counter pulse mode, was the smallest one. Moreover, EL was a useful hemodynamic factor, reflecting the efficiency and hemocompatibility of ECMO. The lower EL meant that less energy was consumed by vascular wall and turbulence, which may result in vascular dysfunction and hemolysis. In this study, the EL, obtained from co-pulse mode ECMO, was more than twofold than that, obtained from constant flow mode and counter pulse mode. That means patients, supported by co-pulse mode ECMO, had higher possibility to suffer from vascular complications and hemolysis. In short, it is demonstrated that the counter pulse mode ECMO could provide better hemodynamic states to the arterial system, which may lead to better outcome to patients.

5 Limitation

The boundary condition, used in this study, was set according to the clinical practice. Hence the results could provide useful information to operator of ECMO and surgeons. However, the results of numerical study was changed by the varied of the boundary condition (including the left ventricular outflow rate and flow rate from ECMO), hence, if the boundary condition is significant different from those reported in this study, the conclusions maybe altered.

6 Conclusion

Numerical studies were conducted to evaluate the hemodynamic differences between constant flow ECMO, co-pulse mode ECMO and counter pulse mode ECMO. Furthermore, this study found that optimal the relationship between left ventricular outflow and ECMO outflow was a viable engineering solution to improve the hemodynamic states and cardiac function. The study results demonstrated that there was more oxygenated blood perfused into the three braches vessels than that under constant flow mode and counter flow mode. That meant the ECMO, working in the counter pulse mode, could provide better oxygen perfusion performance. In addition, the counter pulse mode ECMO could also achieve lowest RRT among the three modes (constant flow mode 220 vs. co-pulse mode 132 vs. counter pulse mode 93), while the peak value of OSI, obtained from the three modes, was similar with each other. Similarly, the results also demonstrated that the ECMO, working under counter pulse mode, could significantly reduce the left ventricular external work (co-pulse mode 1.51 w vs. constant flow mode 1.44 w and counter pulse mode 1.30 w), left ventricular afterload (constant flow mode 1.03 mmHg·s/ml vs. co-pulse mode 1.67 mmHg·s/ml vs. counter pulse mode 0.82 mmHg·s/ml) and energy loss of arterial system (constant flow mode 0.18 w vs. co-pulse mode 0.50 w vs. counter pulse mode 0.16 w). In short, the counter pulse mode ECMO could provide better hemodynamic performance, cardiac function and cerebral oxygen perfusion, compared with that obtained from conventional constant flow ECMO and counter pulse mode ECMO.

Acknowledgment: Funding: This study was partly funded by the National Natural Science Foundation of China (Grant No. 11602007, 91430215, 11572014), BJUT Foundation Fund (Grant No.015000514316007), and Key research and development program (2016YFC0103201, 2017YFC0111104), and New Talent (015000514118002).

Reference

Assmann, A.; Gül, F.; Benim, A. C.; Joos, F.; Akhyari, P. et al. (2015): Dispersive aortic cannulas reduce aortic wall shear stress affecting atherosclerotic plaque embolization. *Artificial Organs*, vol. 39, no. 3, pp. 203-211.

Alwardt, C. M.; Patel, B. M.; Lowell, A.; Lowell, A.; Dobberpuhl, J. et al. (2013): Regional perfusion during venoarterial extracorporeal membrane oxygenation: A case report and educational modules on the concept of dual circulations. *Journal of Extra-corporeal Technology*, vol. 45, no. 3, pp. 187-194.

Adedayo, P.; Wang, S.; Kunselman, A. R.; Ündar, A. (2014): Impact of pulsatile flow settings on hemodynamic energy levels using the novel diagonal medos DP3 pump in a simulated pediatric extracorporeal life support system. *World Journal for Pediatric & Congenital Heart Surgery*, vol. 5, no. 3, pp. 440-448.

Bisdas, T.; Beutel, G.; Warnecke, G.; Hoepfer, M. M.; Kuehn, C. et al. (2011): Vascular complications in patients undergoing femoral cannulation for extracorporeal membrane oxygenation support. *Annals of Thoracic Surgery*, vol. 92, no. 2, pp. 626-631.

Caruso, M. V.; Gramigna, V.; Serraino, G. F.; Renzulli, A.; Fragomeni, G. (2015): Influence of aortic outflow cannula orientation on epiaortic flow pattern during pulsed cardiopulmonary bypass. *Journal of Medical and Biological Engineering*, vol. 35, no. 4, pp. 455-463.

Cheng, Z.; Tan, F. P. P.; Riga, C. V.; Bicknell, C. D.; Hamady, M. S. et al. (2010): Analysis of flow patterns in a patient-specific aortic dissection model. *Journal of Biomechanical Engineering*, vol. 132, no. 5, pp. 1007-1010.

Cheypesh, A.; Yu, X.; Li, J. (2014): Measurement of systemic oxygen consumption in patients during extracorporeal membrane oxygenation-description of a new method and the first clinical observations. *Perfusion*, vol. 29, no. 1, pp. 57-62.

Extracorporeal Life Support Organization (2013): *Extracorporeal Life Support Registry Report: International Summary*. Ann Arbor, MI: ELSO.

Gao, B.; Chang, Y.; Xuan, Y. J.; Zeng, Y.; Liu, Y. J. (2013): The hemodynamic effect of the support mode for the Intra-aorta pump on the cardiovascular system. *Artificial Organs*, vol. 37, no. 2, pp. 157-165.

Goubergrits, L.; Kertzscher, U.; Schoneberg, B.; Wellnhofer, E.; Petz, C. et al. (2008): CFD analysis in an anatomically realistic coronary artery model based on non-invasive 3D imaging: Comparison of magnetic resonance imaging with computed tomography. *International Journal of Cardiovascular Imaging*, vol. 24, no. 4, pp. 411-421.

Guan, Y.; Karkhanis, T.; Wang, S.; Rider, A.; Koenig, S. C. et al. (2010): Physiologic benefits of pulsatile perfusion during mechanical circulatory support for the treatment of acute and chronic heart failure in adults. *Artificial Organs*, vol. 34, no. 7, pp. 529-536.

Gu, K.; Zhang, Y.; Gao, B.; Chang, Y.; Zeng, Y. (2016): Hemodynamic differences between central ECMO and peripheral ECMO: A primary CFD study. *Medical Science Monitor*, vol. 22, pp. 717-726.

He, X. J.; Ku, D. N. (1996): Pulsatile flow in the human left coronary artery bifurcation: Average conditions. *Journal of Biomechanical Engineering*, vol. 118, no. 1, pp. 74-82.

Kabinejadian, F.; Chua, L. P.; Ghista, D. N.; Sankaranarayanan, M.; Tan, Y. S. (2010): A novel coronary artery bypass graft design of sequential anastomoses. *Annals of Biomedical Engineering*, vol. 38, no. 10, pp. 3155-3150.

Khalafvand, S. S.; Ng, E. Y. K.; Zhong, L.; Hung, T. K. (2012): Fluid-dynamics modelling of the human left ventricle with dynamic mesh for normal and myocardial infarction: Preliminary study. *Computers in Biology and Medicine*, vol. 42, no. 8, pp. 863-870.

Lindfors, M.; Frenckner, B.; Sartipy, U.; Bjällmark, A.; Broomé, M. (2017): Venous cannula positioning in arterial deoxygenation during veno-arterial extracorporeal membrane oxygenation-a simulation study and case report. *Artificial Organs*, vol. 41, no. 1, pp. 75-81.

Morbiducci, U.; Gallo, D.; Massai, D.; Ponzini, R.; Deriu, M. A. et al. (2011): On the importance of blood rheology for bulk flow in hemodynamic models of the carotid bifurcation. *Journal of Biomechanics*, vol. 44, no. 13, pp. 2427-2438.

Pinto, S. I. S.; Campos, J. B. L. M. (2016): Numerical study of wall shear stress-based descriptors in the human left coronary artery. *Computer Methods in Biomechanics and Biomedical Engineering*, vol. 19, no. 13, pp. 1443-1455.

Rikhtegar, F.; Knight, J. A.; Olgac, U.; Saur, S. C.; Poulidakos, D. et al. (2012): Choosing the optimal wall shear parameter for the prediction of plaque location-A patient-specific computational study in human left coronary arteries. *Atherosclerosis*, vol. 221, no. 2, pp. 432-437.

Reesink, K. D.; Sauren, L. D.; Dekker, A. L.; Severdija, E.; Nagel, T. V. D. et al. (2005): Synchronously counter pulsating extracorporeal life support enhances myocardial working conditions regardless of systemic perfusion pressure. *European Journal of Cardio-Thoracic Surgery*, vol. 28, no. 6, pp. 790-796.

Sousa, L. C.; Castro, C. F.; António, C. C.; Sousa, F.; Santos, R. et al. (2016): Computational simulation of carotid stenosis and flow dynamics based on patient ultrasound data-A new tool for risk assessment and surgical planning. *Advances in Medical Sciences*, vol. 61, no. 1, pp. 32-39.

Trummer, G.; Foerster, K.; Buckberg, G; Benk, C.; Mader, I. et al. (2014): Superior neurologic recovery after 15 minutes of normothermic cardiac arrest using an extracorporeal life support system for optimized blood pressure and flow. *Perfusion*, vol. 29, no. 2, pp. 130-138.

Wang, S.; Kunselman, A. R.; Clark, J. B.; Üндar, A. (2015): In vitro hemodynamic evaluation of a novel pulsatile extracorporeal life support system: impact of perfusion modes and circuit components on energy loss. *Artificial Organs*, vol. 39, no. 1, pp. 59-66.

Wolfe, R.; Strother, A.; Wang, S.; Kunselman, A. R.; Üндar, A. (2015): Impact of pulsatility and flow rates on hemodynamic energy transmission in an adult extracorporeal life support system. *Artificial Organs*, vol. 39, no. 7, pp. 127-137.

Wen, C. Y.; Yang, A. S.; Tseng, L. Y.; Chai, J. W. (2010): Investigation of pulsatile flow field in healthy thoracic aorta models. *Annals of Biomedical Engineering*, vol. 38, no. 2, pp. 391-402.

Yu, S. C. H.; Liu, W.; Wong, R. H. L.; Underwood, M.; Wang, D. (2016): The potential of computational fluid dynamics simulation on serial monitoring of hemodynamic change in type B aortic dissection. *CardioVascular and Interventional Radiology*, vol. 39, no. 8, pp. 1090-1098.

Zhao, X.; Liu, Y. J.; Bai, F.; Ren, X. C.; Ding, J. L. et al. (2012): Numerical study on bilateral bidirectional glenn shunt. *Journal of Medical Biomechanics*, vol. 27, no. 5, pp. 488-494.

Zhang, Q; Gao, B; Chang, Y. (2018): The numerical study on the effects of cardiac function on the aortic oxygen distribution. *Medical & Biological Engineering & Computing*, vol. 56, no. 7, pp. 1305-1313.